Field measurements of wind pressure on an open roof during Typhoons HaiKui and SuLi

Ruoqiang Feng[*1], Fengcheng Liu[1], Qi Cai[1], Guirong Yan[2] and Jiabing Leng[3]

[1]*School of Civil Engineering, Member of the Key Laboratory of Concrete and Prestressed Concrete Structures of Ministry of Education, Southeast Univ., Nanjing, China*
[2]*Department of Civil, Architectural and Environmental Engineering, Missouri Univ. of Science and Technology, Rolla, MO, USA*
[3]*Zhongnan Construction Group Limited Company, Haimen of Jiangsu province, China*

Abstract. Full-scale measurements of wind action on the open roof structure of the WuXi grand theater, which is composed of eight large-span free-form leaf-shaped space trusses with the largest span of 76.79 m, were conducted during the passage of Typhoons HaiKui and SuLi. The wind pressure field data were continuously and simultaneously monitored using a wind pressure monitoring system installed on the roof structure during the typhoons. A detailed analysis of the field data was performed to investigate the characteristics of the fluctuating wind pressure on the open roof, such as the wind pressure spectrum, spatial correlation coefficients, peak wind pressures and non-Gaussian wind pressure characteristics, under typhoon conditions. Three classical methods were used to calculate the peak factors of the wind pressure on the open roof, and the suggested design method and peak factors were given. The non-Gaussianity of the wind pressure was discussed in terms of the third and fourth statistical moments of the measured wind pressure, and the corresponding indication of the non-Gaussianity on the open roof was proposed. The result shows that there were large pulses in the time-histories of the measured wind pressure on Roof A2 in the field. The spatial correlation of the wind pressures on roof A2 between the upper surface and lower surface is very weak. When the skewness is larger than 0.3 and the kurtosis is larger than 3.7, the wind pressure time series on roof A2 can be taken as a non-Gaussian distribution, and the other series can be taken as a Gaussian distribution.

Keywords: large-span roof; typhoon; full-scale measurements; peak wind pressure; wind pressure spectrum

1. Introduction

Extreme wind pressure values on large-span roofs are important for the wind-load resisting design of the building envelope, and they may be determined on the basis of its probability distribution function (PDF). It is observed that the wind pressure acting on the windward claddings follows a Gaussian distribution, but the wind pressure acting on the roof, especially along the edges and ridges, has been observed to be sometimes non-Gaussian by Tieleman and Ge (2003). Thus, accurate extreme values of the wind pressure on large-span roofs may not be obtained using the Gaussian peak factor. As there were some differences between the extreme values and standard deviations of the wind pressures obtained from models in a wind tunnel and full-scale structures by Apperley (1986), the extreme values and non-Gaussianity of the wind pressure on a large-span roof should be studied with field measurements.

Liu (2017) presents a study on the performance of the moment-based model approach as applied to various non-Gaussian wind pressures on a large-span saddle-type roof. A new strategy is introduced to improve the accuracy of the moment-based model approach, and its effectiveness is examined for various non-Gaussian wind pressures.

Synchronous multi-pressure measurements were carried out for a double-layer reticulated shell roof model in the atmospheric boundary layer wind tunnel by Huang (2016), the existing translated-peak-process (TPP) method had been revised and improved in the estimation of non-Gaussian peak factors, and finally calculated them by employing some various state-of-the-art methods.

The fluctuations of the wind pressure on large-span roofs are discussed little in the literatures. A field study of wind-induced internal pressures in a flexible and porous industrial warehouse with a single dominant opening, of various sizes for a range of moderate wind speeds and directions, was reported by Guha (2013). Pressure measurements were made on erected cantilever roof structures to test the reliability of the wind tunnel tests for predicting pressure distributions on this type of structure by Apperley (1986). Pitsis (1991) compared full-scale and wind tunnel measurements of pressures on built-up Belmore stadium in Sydney, concluding that there were significant differences in the mean and squared deviations of the wind pressure between measurements in wind tunnels and field measurements on the front regions of the roof.

Levitan (1992) and Yeatts (1995) investigated the wind load on low-rise buildings with field measurements on the Texas Tech University experimental low-rise building. Flow visualization of conical vortices on large-span flat roofs was performed in a wind tunnel by Sun *et al.* (2016). The streamline and vorticity field of visual planes on large-span roofs were given by PIV, and they confirmed the influence

---

*Corresponding author, Professor
E-mail: hitfeng@163.com

of wind direction and roof curvature on the appearance of conical vortices. Yoshida (1992) calculated the mean wind pressure coefficient distribution on a membrane roof using a synchronous multi-point scanning system technique. Full-scale measurements were made to investigate wind-induced internal pressures in a high-rise building by Kato (1997), and the suggested internal pressure coefficients in high-rise buildings were provided. The modeling of equivalent static wind loads on low-rise buildings based on full-scale pressure measurements was addressed by Chen (2007). Based on field data from full-scale measurements of a low-rise building during Typhoon Hagupit, the characteristics of the mean, fluctuating and peak pressure coefficients on the leading edges of the roof and the roof-corner regions were investigated by Li (2010). Full-scale measurements of wind actions and wind-induced structural responses of the roof were conducted during the passage of Typhoon Nuri by Chen (2011). The probability density functions of the fluctuating wind pressure on the cantilevered roof were clearly negatively skewed and distinctly deviated from the normal distribution, particularly for the tails. Aly Mousaad (2012) presented an experimental study to assess the wind-induced pressure on full-scale loose concrete roof pavers using the Wall of Wind, a large-scale hurricane testing facility at Florida International University. His study shows that roof pavers could be subjected to significant uplifting wind forces due to negative pressures. Huang (2013) developed a new translated-peak-process method for the estimation of the peak distribution of wind pressure based on the Weibull distribution and point-to-point mapping procedure and verified it in the wind tunnel test of high-rise building. Asmerom (2014) gave a brief review of comparisons between full-scale and University of Western Ontario (UWO) and Tokyo Polytechnic University (TPU) wind tunnel measurements of pressures on the Texas Tech University experimental low-rise building. He suggested that the TPU and UWO pressure simulations are reasonably equivalent and may be used in practice for the design of main wind force resisting systems. Based on field measurements, Shi (2014) investigated some important characteristics and distribution regularities of measured instantaneous wind pressures on a super-tall building during the passage of Typhoon Fanapi.

This paper presents the field measurement results of fluctuating wind load characteristics and extreme pressures on the open roof of WuXi Grand Theater (as shown in Figs. 1 and 2) during Typhoons HaiKui (2012) and SuLi (2013).

2. Field measurement program

2.1 Open roof and monitoring system

WuXi Grand Theater is located in the southern part of the WuLi River. The design wind speed with a return period of 50 years for WuXi is approximately 34.1 m/s at a height of 45 m. WuXi Grand Theater consists of two parts, the covering steel roofs and the covered concrete building, which work separately. Part A of the steel roofs is composed of five leaf-shaped space trusses, named A1, A2, A3, A4

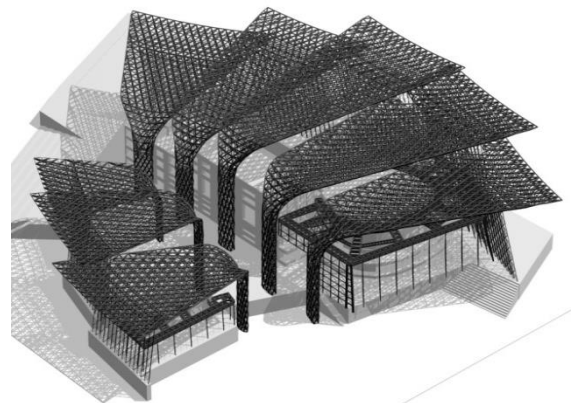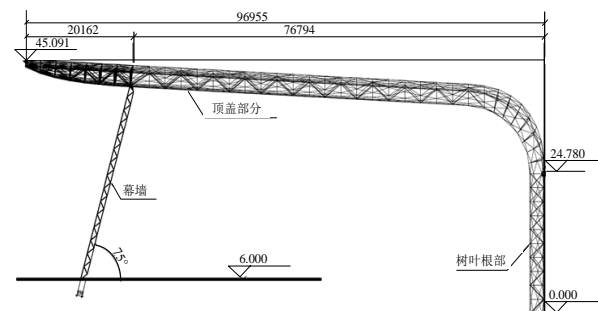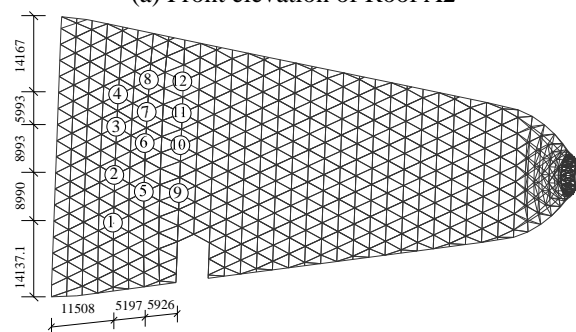Fig. 1 Photograph of WuXi grand theater

Fig. 2 Steel roofs of WuXi grand theater

(a) Front elevation of Roof A2

(b) Top view of Roof A2

Fig. 3 Model of Roof A2

Table 1 Parameters of open roof A2

Span	Width	Sections of chord member pipe	Sections of web member pipe	Yielding stress of pipes
76.79 m	52.28 m	$\Phi350\times10$ (or) $\Phi400\times12$	$\Phi245\times8$ (or) $\Phi328\times8$	345 MPa

and A5, and Part B is composed of three leaf-shaped space trusses, named B1, B2 and B3. The surface of every leaf-shaped space truss is free-form. The wind pressures on the leaf-shaped roof A2 during the typhoons were measured.

The parameters of roof A2 are shown in Fig. 3 and Table 1.

The wind pressure transducer and pressure tap locations are shown in Figs. 4 and 5. The numbers of the taps on upper and lower surface of space truss A2 are 1-12 and 13-24 respectively. The time histories of the wind pressures exerted on the roof were simultaneously acquired at a rate of 40 Hz through an electronically scanned pressure system.

3. Characteristics of fluctuating wind pressures on open roof A2

3.1 Power spectral density of measured wind pressure

The time-histories and power spectral density of the measured wind pressure on Roof A2 during Typhoon HaiKui (8.30 P.M., August 8th, 2012) and Typhoon SuLi (0.30 P.M., July14[th], 2013) are shown in Fig. 6-10, with a sampling time is $25.6\times20= 512$s (with sampling frequency at 40 Hz). There are large pulses in the time-histories of the measured wind pressure. The first wave crest appears near 2 Hz in the power spectral density of the measured wind pressure, and there are many components of medium-high frequencies.

3.2 Spatial correlation coefficients of measured wind pressures

The spatial correlation of the wind pressure affects the gust response of structures. Especially for a structure that is long and has a very low natural frequency, the spatial correlation of wind pressures in the low-frequency range is very important.

(a) on the upper surface
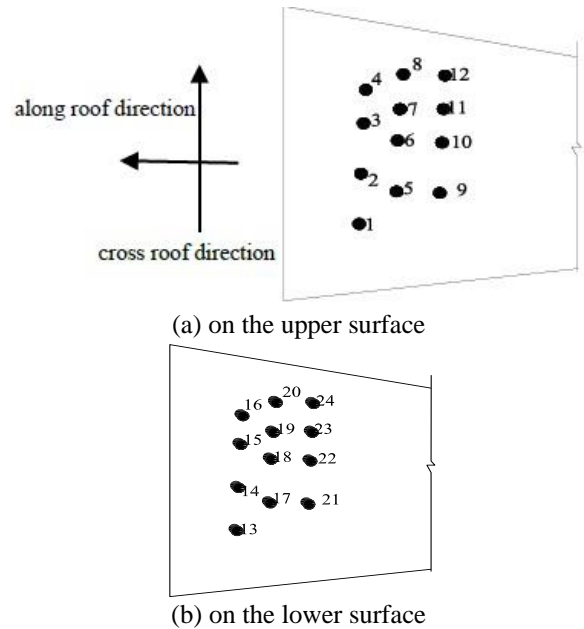

(b) on the lower surface
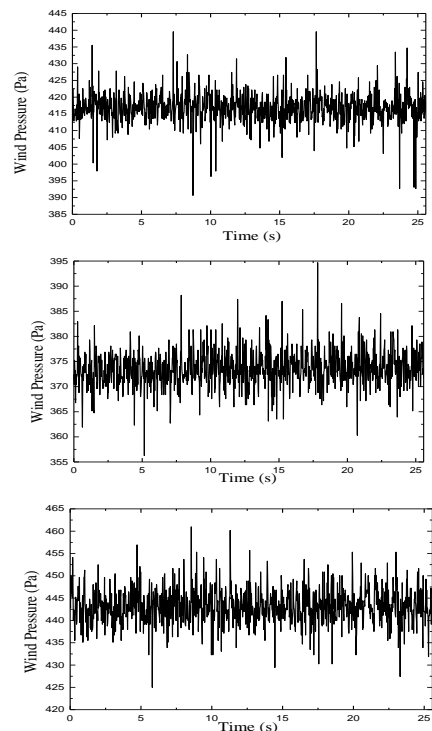
Fig. 5 Locations of pressure taps and definition of wind direction

Fig. 6 Time histories of measured wind pressures of taps 3, 4 and 9 by Typhoon HaiKui at 8.30 P.M., August 8th, 2012
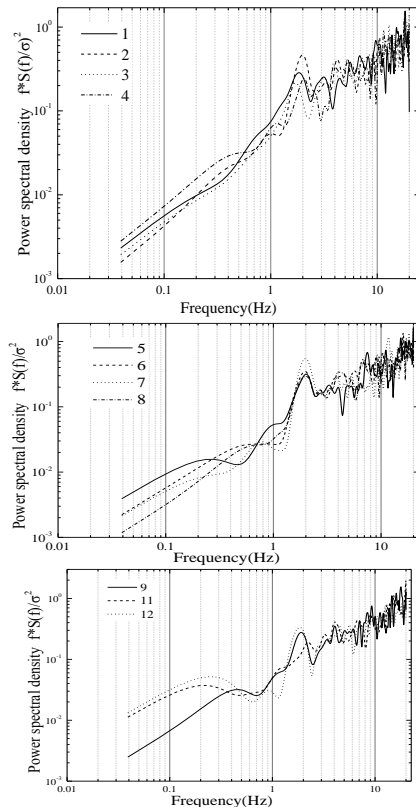

Fig. 4 wind-pressure transducer

Fig. 7 Power spectral densities of measured wind pressures of taps 1-12 by Typhoon HaiKui at 8.30 P.M., August 8th, 2012
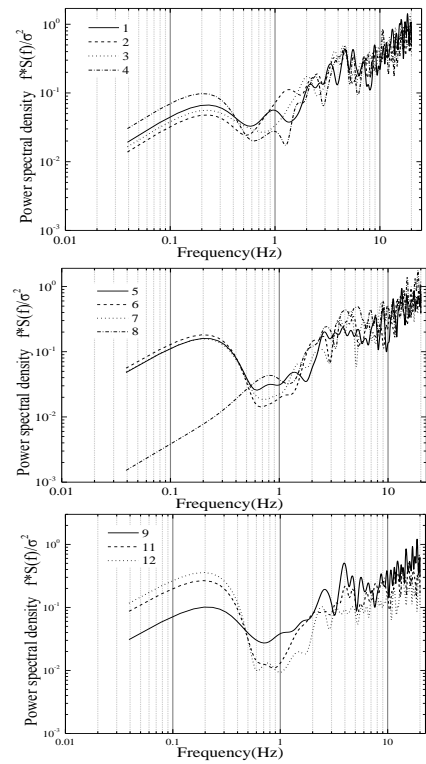

Fig. 9 Power spectral densities of measured wind pressures of taps 1-12 by Typhoon SuLi at 0.30 P.M., July 14th, 2013
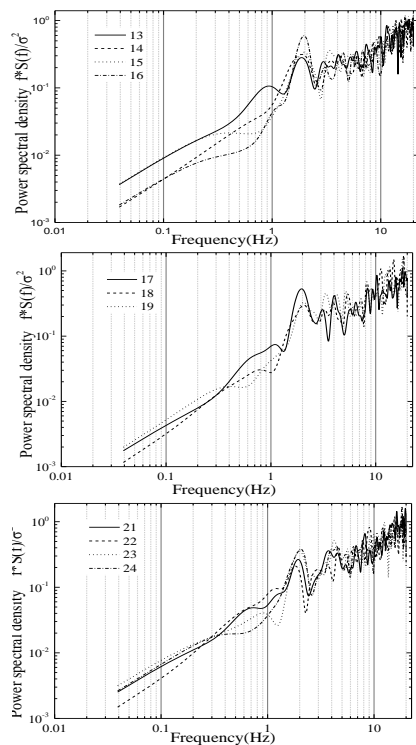

Fig. 8 Power spectral densities of measured wind pressures of taps 13-24 by Typhoon HaiKui at 8.30 P.M., August 8th, 2012
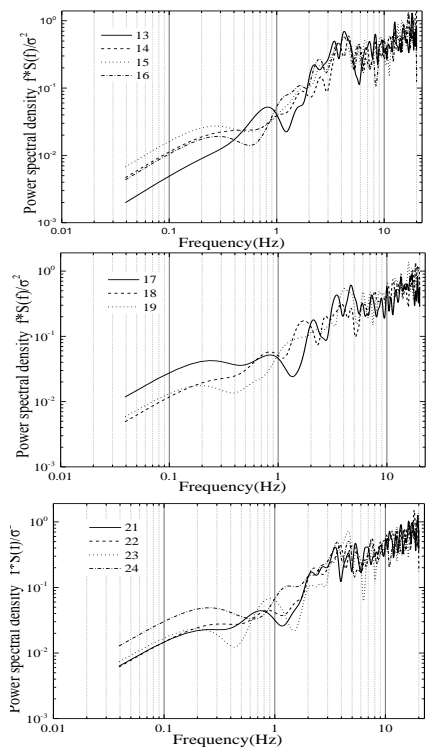

Fig. 10 Power spectral densities of measured wind pressures of taps 13-24 by Typhoon SuLi at 0.30 P.M., July 14th, 2013

Table 2 Sampling times of Typhoons HaiKui and SuLi

Typhoon "HaiKui"	Time 1	Time 2	Time 3	Time 4	Time 5
Time	2012-8-8-20:30	2012-8-8-21:00	2012-8-8-21:30	2012-8-8-22:00	2012-8-8-22:30
Typhoon "SuLi"	Time 6	Time 7	Time 8	Time 9	Time 10
Time	2013-7-14-00:00	2013-7-14-00:30	2013-7-14-01:00	2013-7-14-01:30	2013-7-14-02:30

Table 3 Wind pressure correlation coefficients between corresponding taps on the upper surface and lower surface by Typhoons HaiKui and SuLi

Taps on upper surface(on lower surface)	Time 1	Time 2	Time 3	Time 4	Time 5	Time 6	Time 7	Time 8	Time 9	Time 10
Taps 1(13)	-0.02	-0.06	-0.12	-0.01	-0.10	-0.09	-0.08	-0.04	-0.10	-0.01
Taps 2(14)	0.04	-0.04	-0.02	-0.04	-0.06	0.02	-0.06	-0.03	-0.05	-0.02
Taps 3(15)	-0.05	-0.05	-0.02	-0.01	-0.05	-0.04	-0.01	-0.03	-0.04	-0.03
Taps 4(16)	-0.03	-0.02	-0.05	-0.02	-0.06	-0.01	-0.07	-0.07	-0.05	-0.10
Taps 5(17)	-0.12	-0.09	-0.07	-0.12	-0.02	-0.10	-0.06	-0.07	-0.07	-0.10
Taps 6(18)	-0.04	-0.03	-0.05	-0.11	-0.03	-0.06	-0.09	-0.04	-0.10	-0.06
Taps 7(19)	-0.05	0.00	-0.05	-0.08	-0.05	-0.06	-0.06	-0.07	-0.11	-0.07
Taps 8(20)	0.06	0.03	0.04	0.00	0.02	0.04	0.06	0.08	-0.02	0.04
Taps 9(21)	-0.03	-0.04	-0.05	-0.05	-0.07	-0.07	-0.01	-0.09	-0.01	-0.03
Taps 11(23)	-0.04	-0.02	-0.07	-0.04	-0.10	-0.06	-0.04	0.00	0.00	-0.04
Taps 12(24)	-0.08	-0.10	-0.13	-0.05	-0.15	-0.09	-0.05	-0.10	-0.05	-0.06

Table 4 Wind pressure spatial correlation coefficients of taps on upper surface during Typhoon HaiKui at 8.30 P.M. Aug. 8th, 2012

Tap No.	Tap1	Tap2	Tap3	Tap4	Tap5	Tap6	Tap7	Tap8	Tap9	Tap11	Tap12
Tap1	1.00	-0.02	0.06	-0.09	-0.18	-0.06	-0.10	-0.01	0.06	0.10	0.10
Tap2	-0.02	1.00	-0.17	0.04	-0.08	-0.13	-0.15	-0.14	0.01	0.16	0.13
Tap3	0.06	-0.17	1.00	-0.12	0.00	-0.04	-0.08	-0.07	-0.10	0.09	0.10
Tap4	-0.09	0.04	-0.12	1.00	-0.09	0.08	-0.14	-0.09	-0.08	-0.03	0.05
Tap5	-0.18	-0.08	0.00	-0.09	1.00	0.06	0.09	-0.15	-0.14	-0.06	0.04
Tap6	-0.06	-0.13	-0.04	0.08	0.06	1.00	-0.05	0.15	-0.03	-0.06	-0.05
Tap7	-0.10	-0.15	-0.08	-0.14	0.09	-0.05	1.00	0.00	0.00	-0.13	-0.19
Tap8	-0.01	-0.14	-0.07	-0.09	-0.15	0.15	0.00	1.00	-0.01	-0.08	-0.14
Tap9	0.06	0.01	-0.10	-0.08	-0.14	-0.03	0.00	-0.01	1.00	0.14	-0.14
Tap11	0.10	0.16	0.09	-0.03	-0.06	-0.06	-0.13	-0.08	0.14	1.00	0.04
Tap12	0.10	0.13	0.10	0.05	0.04	-0.05	-0.19	-0.14	-0.14	0.04	1.00

When the spatial correlation is larger than 0.5, it is considered strongly correlated, and when the spatial correlation is less than 0.2, it is weakly correlated. The spatial correlation coefficients between the measured wind pressures of the taps on the upper surface and the corresponding taps on the lower surface of Roof A2 are shown in Table 3, and the sampling times during Typhoon HaiKui and SuLi are shown in Table 2. As shown in Table 3, the spatial correlation of the wind pressures between the upper surface and lower surface is very weak because Roof A2, which is covered by aluminum plates, is windtight. The spatial correlation coefficients of the wind pressures on the upper and lower surface are shown in Tables 4 and 5 respectively. It is indicated that all the absolute values of the spatial correlation coefficients are less than 0.2, and most of the spatial correlation coefficients are less than 0.1 and negative. This is because the taps on Roof A2 are in the middle of the roof and far from the eaves, where the wind pressure varies intensely. The distance between taps on the roof is generally 6.5 m–9 m, so the spatial correlation coefficients of the measured wind pressures on the large-span roof are small.

Table 5 Wind pressure spatial correlation coefficients of taps on lower surface during Typhoon HaiKui at 8.30 P.M. Aug. 8th, 2012

Tap No.	Tap13	Tap14	Tap15	Tap16	Tap17	Tap18	Tap19	Tap21	Tap22	Tap23	Tap24
Tap13	1.00	-0.04	0.11	-0.12	-0.13	-0.12	-0.08	0.03	0.13	0.14	0.06
Tap14	-0.04	1.00	-0.06	-0.02	-0.09	-0.10	-0.10	0.03	0.03	0.19	0.12
Tap15	0.11	-0.06	1.00	0.05	0.03	-0.11	-0.15	-0.08	0.03	0.08	0.24
Tap16	-0.12	-0.02	0.05	1.00	0.15	0.13	-0.22	-0.11	-0.10	0.04	0.13
Tap17	-0.13	-0.09	0.03	0.15	1.00	-0.09	0.10	-0.11	-0.18	-0.11	0.03
Tap18	-0.12	-0.10	-0.11	0.13	-0.09	1.00	-0.14	0.01	-0.13	-0.09	-0.15
Tap19	-0.08	-0.10	-0.15	-0.22	0.10	-0.14	1.00	0.01	0.06	-0.20	-0.15
Tap21	0.03	0.03	-0.08	-0.11	-0.11	0.01	0.01	1.00	-0.16	-0.18	0.10
Tap22	0.13	0.03	0.03	-0.10	-0.18	-0.13	0.06	-0.16	1.00	0.20	-0.25
Tap23	0.14	0.19	0.08	0.04	-0.11	-0.09	-0.20	-0.18	0.20	1.00	0.00
Tap24	0.06	0.12	0.24	0.13	0.03	-0.15	-0.15	0.10	-0.25	0.00	1.00

The spatial correlation coefficients of the taps along the vertical roof direction are shown in Figs. 11 and12. The distribution of the spatial correlation coefficients is the same, and their values fluctuate near zero.
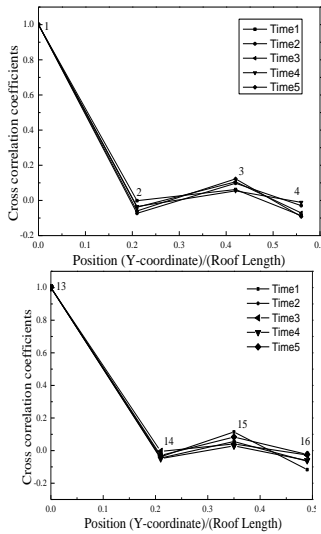

Fig. 11 Spatial correlation coefficients of taps in cross-roof direction
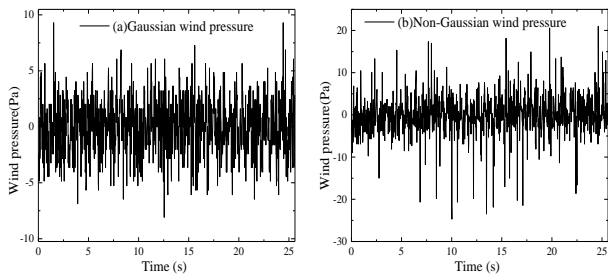
3.3 Non-Gaussian wind pressure characteristics

It is evident that there are some deviations from the Gaussian distribution for the wind pressures measured on Roof A2, with a large amplitude of impulse and asymmetry, as shown in Fig. 12, and the Gaussian distribution has constant values of skewness (0.0) and kurtosis (3.0), which is consistent with the observations previously made by several researchers (e.g., Li *et al.* 1999, Kumar and Stathopoulos 1999, Gioffre *et al*. 2001) that the pressure fluctuations in separated flow regions possess non-Gaussian probability contents.

A process can be classified as having a Gaussian or non-Gaussian history by its skewness and kurtosis, i.e., the third and fourth moments of the normalized history, which are zero and three for a Gaussian history, respectively, as shown in Fig. 13.

The probability plot correlation coefficient (PPCC) method is used to identify the optimum value of the shape parameter that provides the best estimate of the chosen distribution for the time history. To evaluate the suitability of a set of competing distributions for a given set of data, the distribution that generates the maximum PPCC provides the best fit.
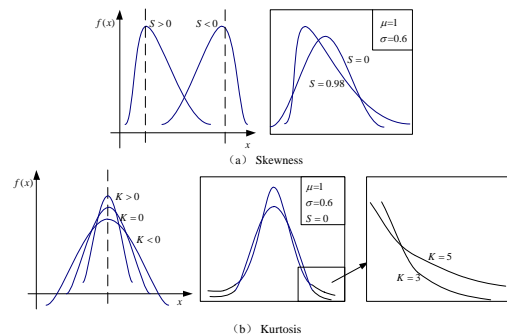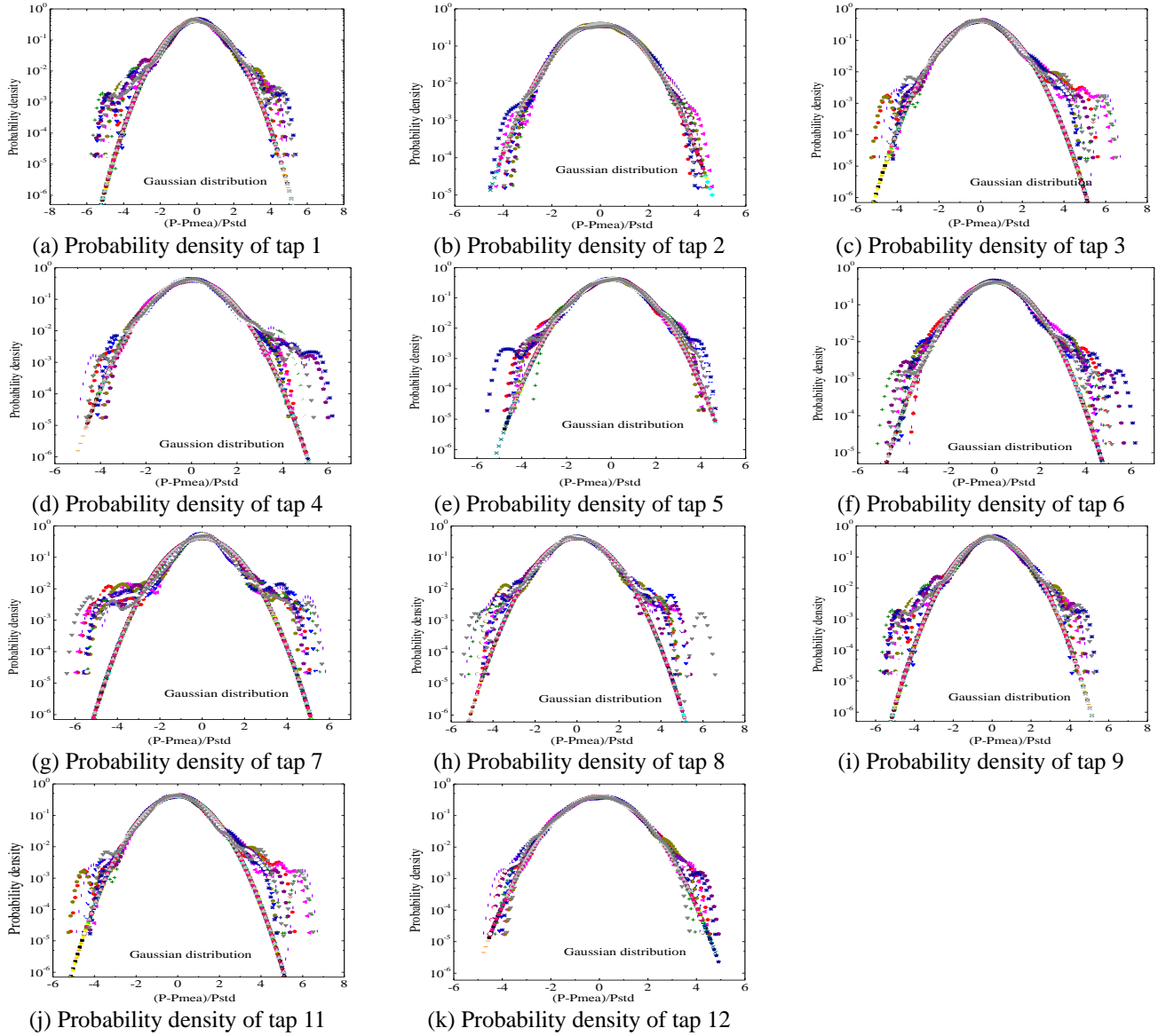

Fig. 12 Field measurements of typical Gaussian and non-Gaussian wind pressures during Typhoon HaiKui

Fig. 13 Non-Gaussian characteristics

(a) Probability density of tap 1

(b) Probability density of tap 2

(c) Probability density of tap 3

(d) Probability density of tap 4

(e) Probability density of tap 5

(f) Probability density of tap 6

(g) Probability density of tap 7

(h) Probability density of tap 8

(i) Probability density of tap 9

(j) Probability density of tap 11

(k) Probability density of tap 12

Fig. 14 Probability density curves of measured wind pressures

The time-histories of the measured wind pressures on space truss A2, shown in Table 2, were used to identify the appropriate probability density function (PDF) of the fluctuating pressure with the probability plot correlation coefficient (PPCC) method, as shown in Fig. 14. The standard normal distribution was also plotted in Fig. 14.

The standardization of the wind pressure $(p - p_{mean})/p_{std}$ was used as the x-coordinate. p_{mean} and p_{std} are the mean value and squared deviation of the wind pressure p, respectively.

Compared with the standard normal distribution, the global symmetry of the probability density curves of the measured wind pressure were adequate, except for taps 3, 4 and 6, whose global asymmetries were large. The skewness of the probability density curves of the measured wind pressure is small, while the difference between the probability density curves of the measured wind pressure

and the standard normal distribution at the end of the probability density curves was slightly larger. The probability density curve of the measured wind pressure was higher than the standard normal distribution, and its kurtosis was larger than 3.0. The relationship between the skewness and kurtosis of all taps is shown in Fig. 15. The range of the kurtosis is between 3 and 8, so the measured wind pressures are the non-Gaussian softening histories.

The skewness in the range between -0.6 and 0.8 was smaller, and most of it was positive.

A quadratic polynomial was used by Dong (2012) to fit the relationship between the skewness and the kurtosis, and the corresponding equations are given in Fig. 15. The range of the skewness of the wind pressures on the flat roofs in the wind tunnel test is between -2 and 1, as determined by Sun (2007). Most of the skewness is negative, and it is larger than that of the measured wind pressure. Moreover, the range of the kurtosis of the wind pressures in the tunnel
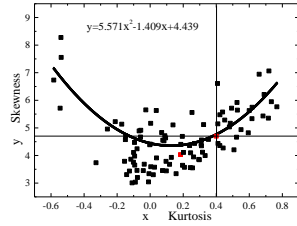
(a) Kurtosis and skewness of taps on the upper surface
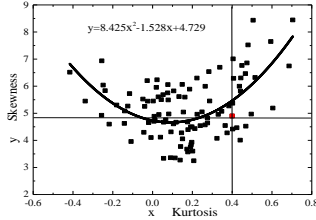
(b) Kurtosis and skewness of taps on the lower surface
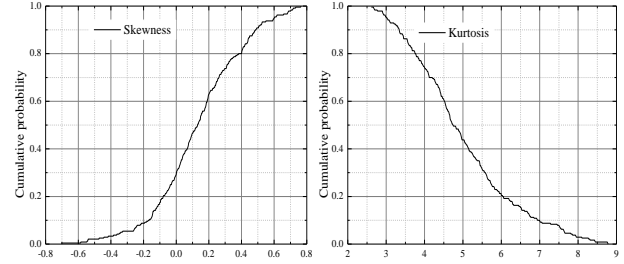
Fig. 15 Fitted curves of kurtosis and skewness
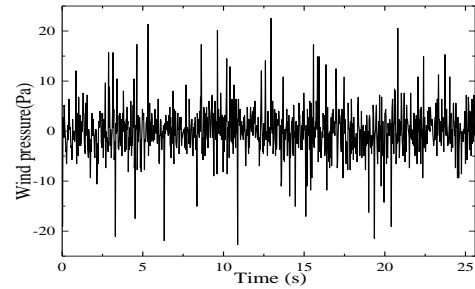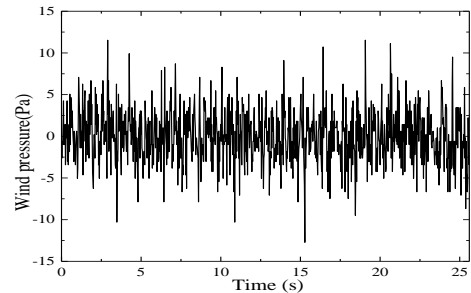

Fig. 16 Cumulative probability curves of skewness and kurtosis
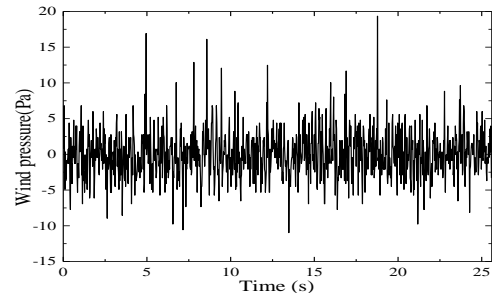

(a) Wind pressure time series of tap 1

(b) Wind pressure time series of tap 3

(c) Wind pressure time series of tap 7 at time 1

(d) Wind pressure time series of tap 7 at time 2

Fig. 17 Typical time series of wind pressure of taps by Typhoon HaiKui

is between 3 and 20 by Dong (2012), which is larger than that of the measured wind pressures in the field. Hence, there is a large difference in the skewness and the kurtosis between wind pressures in the wind tunnel and the measured wind pressures in the field. The reasons are as follows. 1) The model scales are different. As the structural model in the field is a prototype, a small-scale model was used in the wind tunnel. 2) The wind pressure tap locations on roof A2 are in the middle of the roof, at a given distance from the eaves. The taps on the roof models in the wind tunnel test are located in all the positions of the roof, including the separated flow regions and the reattachment regions. Therefore, the skewness and kurtosis of the measured wind pressures in the field are less than those of the wind pressures in the wind tunnel.

3.4 Indication of non-Gaussianity

As an indication, Kumar and Stathopoulos (1999) suggested that a particular region can be considered non-Gaussian if the absolute values of the skewness and kurtosis of the pressure fluctuations on low-rise buildings at various taps are greater than 0.5 and 3.5, respectively. However, the above indication failed at classifying the fluctuating wind pressures on high-rise buildings as Gaussian or non-Gaussian histories, as shown by Gioffre (2001). Instead, maps of the higher-order statistical moments (skewness and kurtosis coefficients) at the four faces of the model of high-rise buildings were proposed by Gioffre (2001) as an easy tool to localize regions with non-Gaussian features and give a measurement of the non-Gaussianity. For large-span spatial roofs, the above measure of the non-Gaussianity is not applicable. Sun (2007) proposed the indication of the non-Gaussianity of fluctuating wind pressures according to the absolute values of the skewness and kurtosis: 1) the absolutevalues of the skewness and kurtosis as an indication should satisfy the fitted curves in Fig. 15; 2) the cumulative probability of the chosen skewness should be close to that of the chosen kurtosis.
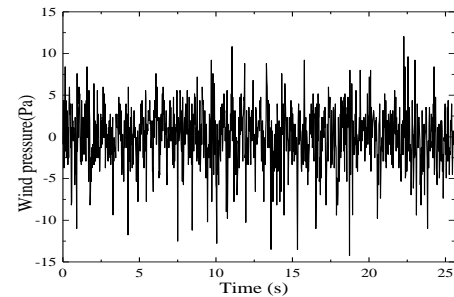
Table 6 First four statistical moments of measured wind pressures in the field by Typhoon HaiKui

Tap No.	Time	Mean	Standard deviation	Skewness	Kurtosis	Distribution
1	Time 1	0	3.49	-0.43	4.74	NG
2	Time 1	0	3.13	0.12	3.68	G
3	Time 1	0	4.67	0.03	7.65	G
4	Time 1	0	3.58	0.08	4.53	G
5	Time 1	0	3.40	0.62	5.75	NG
6	Time 1	0	3.07	0.69	6.21	NG
7	Time 1	0	3.18	-0.04	3.42	G
7	Time 2	0	3.29	0.51	4.74	NG
8	Time 1	0	3.21	0.66	6.95	NG
9	Time 1	0	3.88	-0.15	4.57	G
11	Time 1	0	3.35	0.68	5.43	NG
12	Time 1	0	2.52	-0.01	3.04	G
13	Time 1	0	3.23	0.01	4.70	G
14	Time 1	0	3.01	0.60	5.19	NG
15	Time 1	0	3.28	0.44	6.30	NG
16	Time 1	0	3.26	0.05	2.93	G
17	Time 1	0	2.71	0.02	3.36	G
18	Time 1	0	3.68	0.22	4.96	G
19	Time 1	0	3.80	0.51	8.44	NG
21	Time 1	0	3.39	0.25	5.05	G
22	Time 1	0	3.94	0.15	6.06	G
23	Time 1	0	2.90	0.05	4.07	G
24	Time 1	0	2.91	0.11	4.60	G

Notes: NG is non-Gaussian, G is Gaussian. Mean wind pressures have been subtracted.

According to this indication, the non-Gaussianity of the wind pressures on the flat roofs in the wind tunnel test was shown as $|Skewness| > 0.2, Kurtosis > 3.7$.

As there is a large difference in the skewness and the kurtosis between the wind pressures in the wind tunnel and the measured wind pressures in the field, the indication of Sun (2007) and the accumulative probability of the skewness and kurtosis for the measured wind pressures on open Roof A2 in Fig. 16 have been used to established the new index of the non-Gaussianity of open Roof A2.

Therefore, the proper absolute values of the skewness and the kurtosis for Roof A2 should be confirmed according to the measured fluctuating wind pressures in the field. When $|Skewness| = 0.3, Kurtosis = 4.3$, the accumulative probability of the skewness is close to that of the kurtosis, approximately 70%.

When $|Skewness| > 0.3, Kurtosis > 3.7$, the wind pressure time series can be taken as a non-Gaussian distribution, and the other can be taken as a Gaussian distribution.

The first four statistical moments of the measured wind pressures of the taps on open roof A2 are shown in Table 6 and Fig. 17. It is indicated that 1) the non-Gaussianity has nothing to do with the value of the standard deviation of the fluctuating wind pressure. For examples, the probability

distribution of tap 3, with a large standard deviation, is Gaussian, while the probability distribution of tap 1, with a small standard deviation, is non-Gaussian. 2) The probability distribution of the same tap may change at different times, as in the case of tap 7, which has a probability distribution that is Gaussian at Time 1 but non-Gaussian in at Time 2.

4. Gaussian peak factors using the peak factor method

The extreme values of the wind pressure on large-span roofs are important for the wind-load resisting design of the building envelope. It is observed that the wind pressure acting on the windward claddings follows a Gaussian distribution. Based on the first-crossing probability of Gaussian processes, the method to obtain the extreme value of the wind pressure developed by Davenport (1964) was named the peak factor method and applied in some wind codes and specifications. The equations of Gaussian peak factor are as follow

$$g = \left(2\ln \nu T\right)^{1/2} + \frac{0.5772}{\left(2\ln \nu T\right)^{1/2}} \quad (1)$$

where $\nu = \left\{ \dfrac{\int_0^\infty n^2 S_Y(n)\,d_n}{\int_0^\infty S_Y(n)\,d_n} \right\}^{1/2}$; ν is the effective

frequency; S_Y is the power spectrum of the wind pressure; n is the frequency; T is the observation time ($25.6 \times 20 = 512$ seconds is adopted here, according to the average observing time in field measurements); and 0.5772 is Euler's constant.

Ten different time histories of the wind pressure of each tap were used to obtain the Gaussian peak factor g. The Gaussian peak factors of 22 taps are shown in Fig. 18. The magnitude of the peak factors is found to be approximately 4.2–4.4, with small variation, so the mean Gaussian peak factor $g = 4.3$ can be used as a representative value.

5. Non-Gaussian peak factors using the Hermite moment method

However, the wind pressures acting on the roof, especially along the edges and ridges, have been observed to be generally non-Gaussian (Tieleman 2003), so the accurate extreme values of the wind pressure on large-span roofs cannot be obtained by the Gaussian peak factor. Therefore, two other methods to obtain the extremes value of non-Gaussian wind pressures have been used. One is the Sadek-Simiu method by Sadek and Simiu (2002), and the other is the Hermite moment method presented by Kareem (1994, 1998) and Gurley (1998).

For the Hermite moment method, an explicit translation model called the moment-based Hermite model, in which the shape parameters of the first three-degree Hermite polynomials are determined by the skewness and kurtosis, was adopted. After the non-Gaussian sample is expressed as a monotonic function of a standard Gaussian sample, the extreme value of non-Gaussian sample is mapped onto the Gaussian peak factor.

To establish the probability distribution of the non-Gaussian wind pressure coefficients, the Hermite moment models are adopted to translate the non-Gaussian wind pressure histories into Gaussian histories.
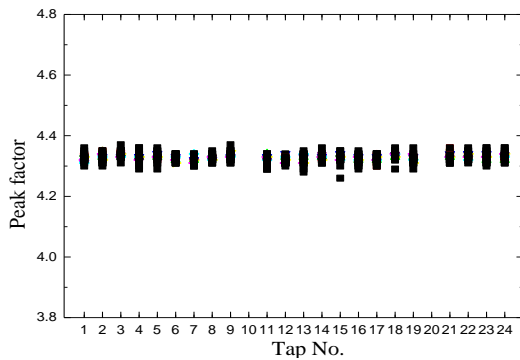

Fig. 18 Gaussian peak factors

The following Hermite polynomial model was established to relate the non-Gaussian process $X(t)$ to a standard Gaussian process $U(t)$ based on its first four moments by Winterstein (1985, 1988).

$$X_0(t) = \frac{X(t) - m_x}{\sigma_X} = \alpha\{U + h_3(U^2 - 1) + h_4(U^3 - 2U)\} \quad (2)$$

where m_x and σ_X denote, respectively, the mean and standard deviation of the wind pressure $X(t)$; $\alpha = (1 + 2h_3^2 + 6h_4^2)^{1/2}$, $h_3 = \dfrac{\gamma_3}{4 + 2\sqrt{1 + 1.5\gamma_4}}$,

$h_4 = \dfrac{\sqrt{1 + 1.5\gamma_4} - 1}{18}$, h_3 and h_4 control the shape of the distribution; $\gamma_3 = \alpha_3$, $\gamma_4 = \alpha_4 - 3$, α_3 is skewness, and α_4 is kurtosis.

The Hermite moment model approach is particularly useful when the probability distribution is unknown but the statistical moments are available. Therefore, following the transformation of random variables, the probability density function can be derived as

$$p_H(X) = \frac{1}{\sqrt{2\pi}} \exp\left[-\frac{U^2(X)}{2}\right] \frac{dU(X)}{dX}$$

where the standardized Gaussian variable $U(X)$ is defined in the following equations

$$U(X) = [\sqrt{\xi^2(X) + c} + \xi(X)]^{1/3} - [\sqrt{\xi^2(X) + c} - \xi(X)]^{1/3} - a$$

, $\xi(X) = 1.5b\left(a + \dfrac{X - m}{\alpha\sigma_X}\right) - a^3$, $a = \dfrac{h_3}{3h_4}$, $b = \dfrac{1}{3h_4}$,

$c = (b - 1 - a^2)^3$.

For a Poisson model, the extreme distribution during the time period T is given as

$$P_{\max}(x) = \exp\left\{-v_0 T \exp\left[-\frac{U^2(X)}{2}\right]\right\} \quad (3)$$

The mean value of the positive extreme values over T can be obtained by

$$\bar{X}_{\max}(X) = \int_0^\infty X\,dP_{\max}(X) = g\sigma \quad (4)$$

where g is called the Gaussian peak factor and σ is the standard deviation of X.

In the linear case of a Gaussian process, the Gaussian peak factor is shown in Eq. (1). For the non-Gaussian case, with the substitution of Eq. (3) into Eq. (4), the mean value of the maximum pressure is given by

$$\bar{X}_{\max}(X) = \int_0^\infty X \exp(-\xi)\,d\xi = g_{NL}\sigma \quad (5)$$

where $\xi = v_0 T \exp\left[-\dfrac{U^2(X)}{2}\right]$, and g_{NL} is the non-Gaussian peak factor. Then, $U(X)$ can be expressed by

$$U(X) = \sqrt{2\ln v_0 T - 2\ln \xi} = \beta - \frac{\ln \xi}{\beta} - \frac{\ln^2 \xi}{2\beta^3} + ... \quad (6)$$

Substituting Eqs. (2) and (6) into Eq. (5) and rearranging, one obtains the following expression for g_{NL}

$$g_{nl} = k\left\{ \left(\beta + \frac{\gamma}{\beta} \right) + h_3 \left(\beta^2 + 2\gamma - 1 \right) + h_4 \left[\beta^3 + 3\beta(\gamma - 1) + \frac{3}{\beta}\left(\frac{\pi^2}{12} - \gamma + \frac{\gamma^2}{2} \right) \right] \right\} \quad (7)$$

where $\beta = \sqrt{2\ln v_0 T}$, $\gamma = 0.5772$.

It is noted that g_{NL} reduces to g when is X is a Gaussian process, i.e., $h_3 = h_3 = 0$ and $k = 1$.

The non-Gaussian peak factors with the Hermite moment method of the wind load pressures are shown in Fig. 19, and their magnitude is approximately 9-13, with high discreteness. The non-Gaussian peak factors with the Hermite moment method are 100% ~ 200% higher than the Gaussian peak factors. Thus, the non-Gaussian peak factors are very important for determining the extreme values of the wind pressures on the building envelope. Referring to Fig. 19, the Hermite moment method may exaggerate the extreme values of the non-Gaussian wind pressure on Roof A2.

6. Non-Gaussian peak factors using the Sadek-Simiu method

6.1 Sadek-Simiu method

A procedure developed by Sadek and Simiu (2002) can be employed to obtain the distribution of the peak pressure and load coefficients from a single sample record. This new procedure is especially useful for external surface pressures and surface loads that are generally not normally distributed. The procedure permits the design of wind-load-sensitive parts to be based on more accurate information and should therefore be more reliable than the methods currently available with the provisions of the building code.
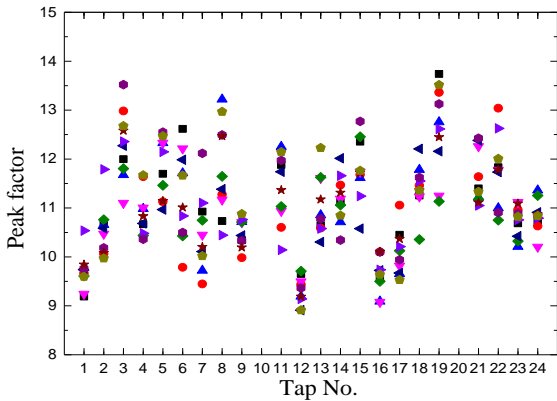
Fig. 19 Non-Gaussian peak factors using the Hermite moment method

The preliminary step for this new procedure is to identify the appropriate probability density function (PDF) of the parent time history that represents either the fluctuating pressure or the load coefficients. The probability plot correlation coefficient (PPCC) method is used to identify the optimum value of the shape parameter that provides the best estimate of the chosen distribution for the time history. To evaluate the suitability of a set of competing distributions for a given set of data, the distribution that generates the maximum PPCC provides the best fit.

The general expression for the PDF of this three-parameter gamma distribution is

$$f(y) = \frac{\left(\frac{x - \mu}{\beta} \right)^{\gamma - 1} e^{-(x-\mu)/\beta}}{\beta \Gamma(\gamma)} \quad x > \mu$$

where β, γ and μ = scale, shape, and location parameter, respectively, and $\Gamma() = $ gamma function.

Once the appropriate marginal probability distributions are obtained, the following procedure for estimating peak statistics, based on a translation processes approach, is followed. Consider a stationary non-Gaussian time series $x(t)$ with marginal distribution $f_X(x)$ and duration T. This process is mapped onto a time series $y(t)$ with a standardized marginal normal distribution $F_Y(y)$. For the process $y(t)$, the cumulative distribution function (CDF) of the largest peak during time interval T is obtained using classical results (Rice 1954).

$$F_{Y_{pk,T}}(y_{pk,T}) = \exp[-v_{0,y}T\exp(-y_{pk,T}^2/2)] \quad (8)$$

where $v_{0,y}$ is the zero upcrossing rate of the Gaussian process $y(t)$, $v_{0,y} = \sqrt{\dfrac{\int_0^\infty n^2 S_y(n)dn}{\int_0^\infty S_y(n)dn}}$.

In practice, it is assumed that $S_y(n)$ may be replaced by the spectral density function of process $x(t)$, $S_x(n)$. For the spectral density shapes of the general type considered in this paper, the errors inherent in this assumption have been verified to be negligible (Grigoriu 1995).

For a specified cumulative probability $F_{Y_{pk,T}}$, the above equation yields the corresponding maximum and minimum peaks of

$$y_{pk,T}^{\max} = \sqrt{2\ln\frac{-v_{0,y}T}{\ln F_{Y_{pk,T}}}} \quad \text{and} \quad y_{pk,T}^{\min} = -\sqrt{2\ln\frac{-v_{0,y}T}{\ln F_{Y_{pk,T}}}}$$

Once the cumulative distribution function of the largest peaks is determined from Eq. (8), the distribution of the largest peaks of $x(t)$ is estimated by mapping the peaks of the normally distributed time series on the non-Gaussian distribution space (Grigoriu 1995, Gioffre *et al.* 2001).

The procedure is illustrated in Fig. 20, where for a given

cumulative probability of the peaks, $F_{Y_{pk}}(y_{pk})$, the Gaussian peak effect, y_{pk}, and its cumulative probability in the Gaussian space, $F_Y(y)$, are determined. The corresponding peak in the non-Gaussian space, x_{pk}, is then estimated, corresponding to a cumulative probability of $F_{x_{pk}}(x_{pk}) = F_{y_{pk}}(y_{pk})$.

a) select a value $F_{y_{pk}}'$ between zero and one.

b) find the corresponding value y_{pk} and

c) the corresponding value $F_y'(y)$

d) with $F_x^{\Leftrightarrow}(x) = F_y(y)$, determine the corresponding value of $x(t)$.

e) for the same value $x = x_{pk}$ and the intersection with the line $F_{x_{pk}}(x_{pk}) = F_{y_{pk}}(y_{pk})$, one point on the CDF of the peak distribution of $x(t)$ is obtained.

Repeat the above steps for different values of $F_{y_{pk}}'(y_{pk})$ to generate the CDF of the peaks of $x(t)$. According to the definition of the peak factor, the non-Gaussian peak factor g is

$$g = \frac{x_{max}}{\sigma} \qquad (9)$$

6.2 Non-Gaussian peak factors

Ten different time histories of the wind pressure of each tap (the same as the above two methods) are used to obtain the non-Gaussian peak factor g using the Sadek-Simiu method and guaranteed rates of 85%, 90%, 95% and 99.5%, as shown in Fig. 21. The non-Gaussian peak factors of the same taps with different guaranteed rates are different, as are the non-Gaussian peak factors of different taps with the same guaranteed rate. Therefore, it is not accurate to address different taps using the same peak factor.
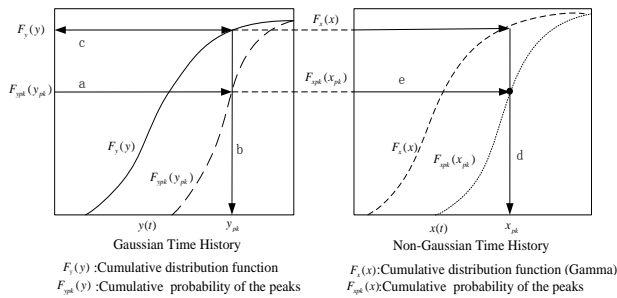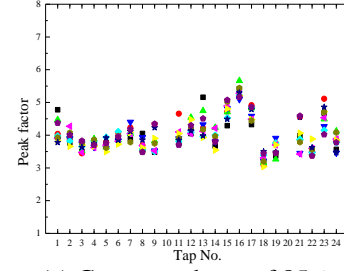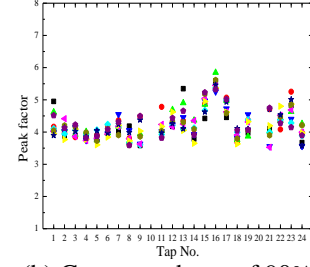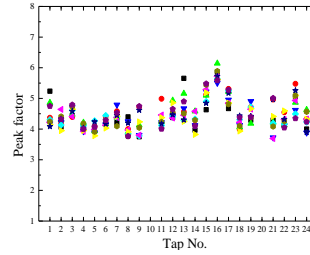

Fig. 20 Mapping procedure for a point from a non-Gaussian process $x(t)$ to a Gaussian process $y(t)$
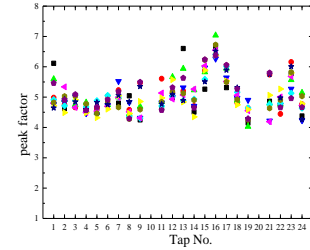

(a) Guaranteed rate of 85%

(b) Guaranteed rate of 90%

(c) Guaranteed rate of 95%

(d) Guaranteed rate of 99.5%

Fig. 21 Non-Gaussian peak factors with Sadek-Simiu method

As shown in Fig. 21(d), the range of the non-Gaussian peak factors with the guaranteed rate of 99.5% is between 4.0~7.0, and the average value of the non-Gaussian peak factors is 5.01. The range of the non-Gaussian peak factors of the same tap with different time histories is less than that of the peak factors of different taps with the same time history. The non-Gaussian peak factors with the Sadek-Simiu method are larger than the Gaussian peak factors with the peak factor method, which are near the lower limiting value of the non-Gaussian peak factors.

7. Peak factors of field measurements of wind pressure on open Roof A2

The peak factors of the above three methods are shown in Fig. 22. It is indicated that 1) the Gaussian peak factors are evenly distributed, and the difference between different
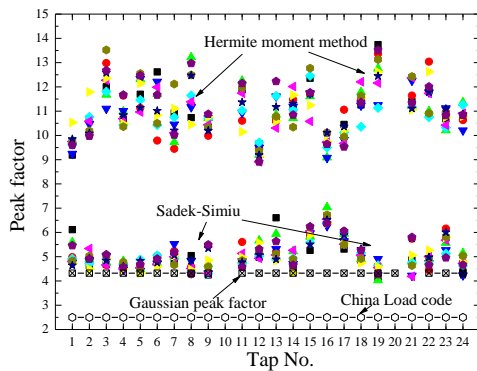
Fig. 22 Comparison of peak factors obtained using the three methods

times is small, so their value can be approximately established as $g \approx 4.3$; 2) the peak factors with the Sadek-Simiu method at a guaranteed rate of 99.5% are slightly larger than the Gaussian peak factors; 3) the range of the peak factors with the Hermite moment method is 9~13; the peak factors change greatly at different times and are 100%~200% larger than those obtained using the other two methods.

The peak factors with the Hermite moment method show a highly discrete distribution and are much larger than those with the other two methods. Hermite moment method may exaggerate the non-Gaussianity and may be not applicable in evaluating the measured peak wind pressure on the WuXi grand theater in the field. According to the analysis of the peak factors with the above three methods, the values of the non-Gaussian peak factors of Roof A2 of the Wuxi grand theater can be established as approximately $g \approx 4.65$, which is far larger than the usual peak factor $g_u = 2.5$ specified in the Load code for the design of building structures in China GB50009-2012.

8. Conclusions

• During Typhoon HaiKui (August 8th, 2012) and Typhoon SuLi (July14th, 2013), there were large pulses in the time-histories of the measured wind pressure on Roof A2 in the field. The first wave crest appears near 2 Hz in the power spectral density of the measured wind pressure, and there are many components of medium-high frequencies.
• The spatial correlation of the wind pressures on roof A2 between the upper surface and lower surface is very weak because roof A2, covered by aluminum plates, is windtight. The wind pressure spatial correlation coefficients on roof A2 are less than 0.2, and most of the spatial correlation coefficients are less than 0.1 and negative. This is because the taps on Roof A2 are in the middle of the roof, far from the eaves, where the wind pressure varies intensely. The distance between taps on the roof is generally 6.5 m–9 m.

• The probability density curve of the measured wind pressures on roof A2 is higher than the standard normal distribution, and its kurtosis is larger than 3.0. The range of the kurtosis is between 3 and 8, so the measured wind pressures have non-Gaussian softening histories. The skewness has a smaller range between -0.6 and 0.8, and most of it is positive.
• The relationship between the skewness and the kurtosis can be approximately fitted with a quadratic polynomial. When $|Skewness| > 0.3, Kurtosis > 3.7$, the wind pressure time series on roof A2 can be taken as a non-Gaussian distribution, and the other series can be taken as a Gaussian distribution.

References

Aly, A.M., Bitsuamlak, G.T. and Chowdhury, A.G. (2012), "Full-scale aerodynamic testing of a loose concrete roof paver system", *Eng. Struct.*, **44**, 260-270.

Apperley, L.W. and Pitsis, N.G. (1986), "Model/full-scale pressure measurements on a grandstand", *J Wind Eng Ind Aerod.*, **23**, 99-111.

Chen, F., Li, Q.S. and Wu, J.R. (2011), "Wind effects on a long-span beam string roof structure: Wind tunnel test, field measurement and numerical analysis", *J. Constr. Steel Res.*, **67**(10), 1591-1604.

Chen, X. and Zhou, N. (2007), "Equivalent static wind loads on low-rise buildings based on full-scale pressure measurements", *Eng. Strut.*, **29**(10), 2563-2575.

Chinese Ministry of Construction (2012), "Load code for the design of building structures in China", *GB50009-2012, Beijing, China.*

Davenport, A.G. (1964), "Note on the distribution of the largest value of a random function with application to gust loading", *Proc. Inst. Civil. Eng.*, (28), 187-196.

Dong, X. (2012), "Research of wind loads on saddle and flat roofs induced by destructive vortices", Ph.D. Dissertation, *Southeast University*, *NanJing.*

Gioffrè, M., Gusella, V. and Grigoriu, M. (2001), "Non-Gaussian wind pressure on prismatic buildings. I: Stochastic field", *J Struct. Eng. -ASCE*, **127**(9), 981-989.

Gioffrè, M., Gusella, V. and Grigoriu, M. (2001), "Non-Gaussian wind pressure on prismatic buildings. I: Stochastic field", *J. Struct. Eng. -ASCE*, **127**(9), 981-989.

Grigoriu, M. (1995), *Applied Non-Gaussian Processes: Examples, Theory, Simulation, Linear Random Vibration, and MATLAB Solutions,* Prentice Hall. New Jersey.

Guha, T.K., Sharma, R.N. and Richards, P.J. (2013), "Field studies of wind induced internal pressure in a warehouse with a dominant opening", *Wind Struct.*, **16**(1), 117-136.

Gurley, K.R. and Kareem, A. (1998), "A conditional simulation of non-normal velocity/pressure fields", *J. Wind Eng. Ind. Aerod.*, **77**, 39-51.

Hagos, A., Habte, F. and Chowdhury, A.G. (2014), "Comparisons of two wind tunnel pressure databases and partial validation against full-Scale measurements(online)", *J. Struct. Eng. -ASCE*, **140**(10).

Huang, M.F., Huang, S., Feng, H., et al. (2016), "Non-Gaussian time-dependent statistics of wind pressure processes on a roof structure". *Wind Struct.*, **23**(4), 275-300.

Huang, M.F., Lou, W., Chan, C.M., Lin, N. and Pan, X. (2013), "Peak distributions and peak factors of ind-induced pressure processes on tall buildings", *J Eng. Mech. -ASCE*, **139**(12), 1744-1756.

Kareem, A. and Zhao, J. (1994), "Analysis of non-Gaussian surge response of tension leg platforms under wind loads", *J. Offshore Mech. Arct.*, **116**(3),137-144.

Kato, N., Niihori, Y. and Kurita, T. (1997), "Full-scale measurement of wind-induced internal pressures in a high-rise building", *J. Wind Eng. Ind. Aerod.*, **69**, 619-630.

Kumar, K.S. and Stathopoulos, T. (1999), "Synthesis of non-Gaussian wind pressure time series on low building roofs", *Eng. Struct.*, **21**(12), 1086-1100.

Levitan, M.L. and Mehta, K.C. (1992), "Texas tech field experiments for wind loads part 1: building and pressure measuring system", *J. Wind Eng. Ind. Aerod.*, **43**(1), 1565-1576.

Li, Q., Dai, Y. and Li, Z. (2010), "Wind pressures on low-rise building surface during a severe typhoon 'Hagupit' ", *J. Build. Struct.*, **31**(4), 62-68

Li, Q.S., Calderone, I. and Melbourne, W.H. (1999), "Probabilistic characteristics of pressure fluctuations in separated and reattaching flows for various free-stream turbulence", *J. Wind Eng. Ind. Aerod.*, **82**(1), 125-145.

Liu, M., Chen, X. and Yang, Q. (2017), "Estimation of peak factor of non-Gaussian wind pressures by improved moment-based Hermite model". *J. Eng. Mech. -ASCE*, **143**(7).

Pitsis, N.G. and Apperley, L.W. (1991), "Further full-scale and model pressure measurements on a cantilever grandstand", *J Wind Eng. Ind. Aerod.*, **38**(2), 439-448.

Rice, S.O. (1954), "Mathematical analysis of random noise", *Bell Syst. Technical J.*, **23**(3), 282-332.

Sadek, F. and Simiu,. E. (2002), "Peak non-Gaussian wind effects for database-assisted low-rise building design", *J. Eng. Mech. - ASCE*, **128**(5), 530-539.

Shi, W., Li, Z. and Luo, D. (2014), "Comparison of field measurement and wind tunnel test of wind pressure characteristics over super-tall building during the passage of typhoon Fanabi", *ACTA Aerodynamica Sinica,* **32**(2), 264-271.

Sun, H. and Ye, J. (2016), "3-D characteristics of conical vortex around large-span flat roof by PIV technique", *Wind Struct.*, **22**(6), 663-684.

Sun, Y., Wu, Y. and Lin, Z. (2007), "Non-Gaussian features of fluctuating wind pressures on long span roofs", *China Civil. Eng. J.*, **40**(4), 1-5.

Tieleman, H.W., Ge, Z., Hajj, M.R. and Reinhold, T.A. (2003), "Pressures on a surface-mounted rectangular prism under varying incident turbulence", *J Wind Eng. Ind. Aerod.*, **91**(9), 1095-1115.

Winterstein, S.R. (1985), "Non-normal responses and fatigue damage", *Struct. Eng. -ASCE*, **111**(10), 1291-1295.

Winterstein, S.R. (1988), "Nonlinear vibration models for extremes and fatigue", *J. Eng. Mech. - ASCE*, **114**(10), 1772-1790.

Yeatts, B.B., Mehta, K.C. and Smith, D.A. (1995), "Field experiments for wind effects on low buildings", *Proceedings of the 9th Int. Conf. on Wind Engineering*.

Yoshida. M., Kondo, K. and Suzuki, M. (1992), "Fluctuating wind pressure measured with tubing system", *J. Wind Eng. Ind. Aerod.*, **42**(1), 987-998.

CC